

Characterization of Phase Transformations During Graded Thermo-Mechanical Processing of Press-Hardening Sheet Steel 22MnB5



A. REITZ, O. GRYDIN, and M. SCHAPER

Safety-relevant components in automobiles require materials that combine high strength with sufficient residual ductility and high-energy absorption. A graded thermo-mechanical treatment of the press-hardening steel 22MnB5 with graded microstructure can provide a material with such properties. Different austenitization temperatures, cooling and forming conditions within a sheet part lead to the development of microstructures with mixed phase compositions. To determine the resulting phase contents in such graded processed parts, a large number of dilatometric tests are usually required. With a non-contact characterization method, it is possible to detect local phase transformations on an inhomogeneously treated flat steel specimen. For press-hardening steel after heat treatment and thermo-mechanical processing, correlations between austenitization temperature, hot deformation strain, microstructure, and hardness are established.

<https://doi.org/10.1007/s11661-020-05976-x>
© The Author(s) 2020

I. INTRODUCTION

DUE to their advantageous specific properties such as a high strength combined with a sufficient residual deformability and a high-energy absorption in the event of a crash, press-hardened components find increasing use in the automotive industry.^[1] The martensitic microstructure of a press-hardened part, which reaches tensile strengths of up to 1500 MPa, develops during the simultaneous forming and quenching in cooled dies.^[2] While a cooling rate above the critical rate of 25 K/s is required for the formation of a fully martensitic microstructure according to the continuous cooling transformation (CCT) diagram of 22MnB5, softer phases such as ferrite, pearlite, and bainite are formed at lower cooling rates.^[3] The formation of these phases is influenced by hot deformation, whereby a shift of the ferritic and bainitic area to shorter times has been observed at a hot deformation degree of 20 or 40 pct.^[4–6] A specific adjustment of a mixed microstructure can produce a material with both high strength and elongation, for which phase compositions of martensite and bainite or martensite and ferrite are favorable.^[7]

The process route of direct press hardening generally consists of austenitizing, hot forming, and quenching the parts.^[5] A diffusional transformation of austenite into ferrite or bainite is preferred in non-isothermally deformed boron steels according to Shi *et al.*, which also resulted in a lower martensite start temperature M_s .^[8] Zhou *et al.* found that austenitization at a temperature of 800 °C or 850 °C leads to a microstructure consisting of undissolved pearlite, fragmentary ferrite, and martensite.^[9] Press-hardened parts made of 22MnB5 reach hardness values of 450 HV, which is 50 HV lower compared to water quenched 22MnB5 parts due to a self-tempering of martensite.^[10] The crash performance of body in white components produced by press hardening is related to the microstructure of the parts.^[7] Furthermore, this microstructure is dependent on the deformation temperature and strain, the cooling rate, the initial grain size, the chemical composition, *etc.*^[6] In order to achieve an optimum modification of the mechanical properties of multiphase steels, knowledge of the phase compositions and the morphology of the individual phases is essential.^[11]

In addition, tailored hot formed parts are produced by press hardening with areas of lower strength but higher ductility to improve the crashworthiness of the part.^[1,2] To reach such tailored properties in one component, different heating or cooling paths are applied within particular blank regions.^[2] The data on the change in phase transformation kinetics as a function of thermal and strain conditions are of primary importance for the correct design of tailored microstructures with an optimal morphology.^[11]

A. REITZ, O. GRYDIN, and M. SCHAPER are with the Department of Material Science, Paderborn University, Warburger Straße 100, 33098 Paderborn, Germany. Contact e-mail: grydin@lwk.upb.de

Manuscript submitted June 4, 2020.

Article published online September 18, 2020

When monitoring phase transformations of steels, changes in the lattice structure and specific volume can be detected.^[12] If a phase transformation has occurred, it can be recognized as a small deviation of the cooling curve due to its exothermal nature.^[13] Dilatometry, differential thermal analysis, and differential scanning calorimetry are methods for detecting phase transformations.^[14] The determination of a resulting mixed microstructure for a graded component by dilatometry would lead to both a high number of dilatometer tests and a high experimental effort, because the tests use nearly homogeneous thermal and strain states within a specimen.

The purpose of this study is to use a contactless characterization method for the analysis of phase transformations during the graded thermo-mechanical processing of sheet material using the example of press-hardening steel 22MnB5. This new method made it possible to determine the influence of different austenitization temperatures on the phase transformation kinetics with a single specimen. High-temperature digital image correlation (DIC) and thermal imaging were used for the detection of the phase transformations.

II. EXPERIMENTAL PROCEDURE

For the high-temperature DIC tests, uncoated 22MnB5 specimens with a thickness of 1.5 and 2 mm were cut along the rolling direction of the sheet by wire cut EDM. The chemical composition of the steel sheets, which were determined by spark spectroscopy with Q4 TASMAN from Bruker AXS GmbH, is presented in Table I.

Figure 1 shows the test setup for the high-temperature DIC tests. A high-frequency generator from Trumpf Hüttinger with a maximum power of 10 kW and a frequency of 250 kHz was used to heat the flat steel specimens with a frontal inductor equipped with a surrounding U-shaped flux concentrator. It allows fast heating of the samples up to 900 °C. A gradation of the specimen temperature is achieved by a targeted use of the frontal inductor in the upper region of the specimen (see Figure 1).

The images for the DIC evaluation were taken with a Nikon D3200, and the infrared thermal imaging camera VarioCAM® HD head 980 from Infratec was used to record the temperature change during the heat treatments. The recording frequency of both cameras was 1 Hz. A temperature measurement range of 250 °C to 2000 °C was utilized. For the DIC tests, the cleaned specimens were completely covered with a black high-temperature varnish and the white speckle pattern was applied with a white high-temperature varnish. The dog-bone shaped flat specimens are 178 mm long and 8 mm wide in the narrow section. An emission coefficient of 0.95 for the thermal imaging camera was determined by a comparative measurement with a ratio pyrometer.

In all tests, the specimens were heated to austenitization temperatures between 800 °C and 900 °C, using the inductor installed behind the rear specimen surface with

a coupling distance of 2 mm. The software GOM Correlate was used to determine the local strain evolution during the cooling of the specimens. The temperature and strain development was measured simultaneously during soaking and cooling on the front specimen surface by means of the thermal imaging and the digital camera. To eliminate the influence of sample radiation at high temperatures, an optical bandpass filter was applied. In addition, an optional tensile deformation was performed after heating to the austenitization temperature within 60 seconds and soaking for 10 to 300 seconds at a tension speed of 1 mm/s until a total elongation of 10 or 20 pct was reached. The non-deformed samples underwent the same temperature ramp. The specimens were then cooled to the ambient temperature in free air or quenched by compressed air. Afterwards, the specimens for the hardness tests and metallographic analyses were taken. The data from the thermal imaging camera were transferred to the GOM Correlate software, in which the entire specimen surface could be analyzed and the strain and temperature changes could be compared. Three temperature ranges (800 °C, 850 °C, and 900 °C) were investigated for each specimen to examine the influence of different austenitization temperatures on phase transformations during heat treatment and thermo-mechanical processing (Figure 2). After calculating the cooling rate of each area of interest according to Eq. [1],^[14] the average cooling rates for the three areas were determined for each specimen. The automatic hardness tester KB 30 FA was utilized to test the hardness, and the measurements were carried out with a force of 9.807 N (HV1). The polished specimens were etched according to Lepera to create micrographs.^[15] These were then examined with the digital light microscope Keyence VHX5000 and the scanning electron microscope (SEM) Zeiss Ultra Plus. The SEM was operated at an acceleration voltage of 20 kV with a secondary electron detector or in-lens detector.

$$\text{cooling rate} = \frac{300 \text{ }^{\circ}\text{C}}{t8/5} \quad [1]$$

with $t8/5$ time taken for cooling from 800 °C to 500 °C.

The general experimental design for the heat treatment and the thermo-mechanical treatment of the flat steel specimens is presented in Table II.

Diagrams, as shown in Figure 3, were created to identify the beginning and end of the phase transformations. The $D\phi_y/DT$ curve shows the change in strain and temperature as a function of time for a region of interest. If this curve deviates from the usually horizontal course of the graph and if there are additional deviations from the otherwise smooth cooling curve, a phase transformation took place.

The green $D\phi_y/DT$ curve for area 2 and the corresponding green temperature curve show no significant differences, indicating that no phase transformation occurred. According to the CCT diagram in Reference 3, area 2 was heated below the Ac_1 temperature, which implies that no phase transformations could take place during cooling. The blue $D\phi_y/DT$ curve displays a

Table I. Initial Grain Size and Chemical Composition of the 22MnB5 Flat Steel Sheets

Thickness (mm)	Initial Grain Size (μm)	C Pct	Si Pct	Mn Pct	Cr Pct	B Pct	Ti Pct	Fe Pct
1.5	6.88	0.219	0.200	1.185	0.193	0.0020	0.027	97.95
2.0	7.65	0.236	0.218	1.188	0.181	0.0022	0.025	97.95

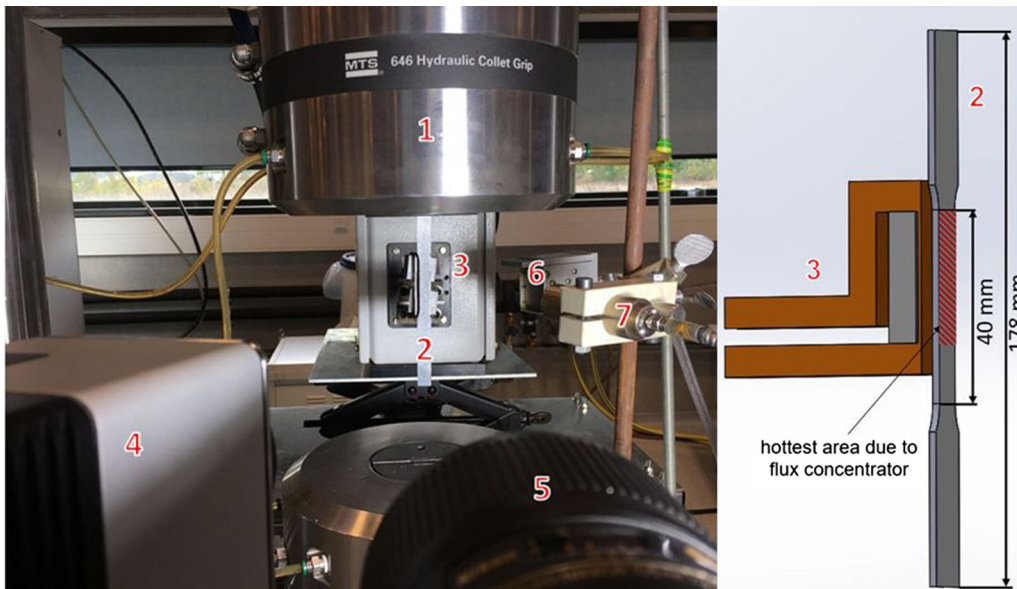


Fig. 1—Experimental setup for the characterization of phase transformations: (1) chuck jaws of a hydraulic universal testing machine, (2) specimen, (3) medium frequency oscillator with frontal inductor in combination with a magnetic flux concentrator, (4) thermal imaging camera, (5) digital camera, (6) air nozzle, (7) ratio pyrometer.

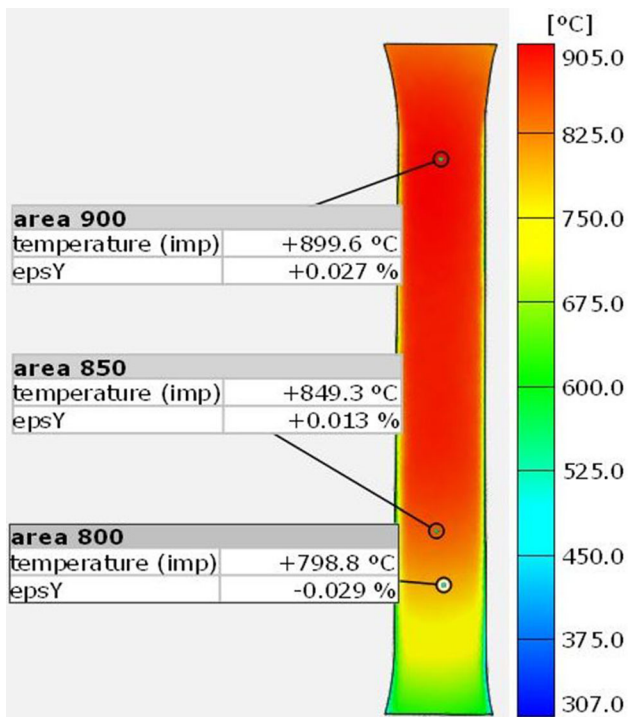


Fig. 2—Thermal image of a graded heat-treated specimen.

deviation, with the start and end of the peak representing the start and end of a phase transformation. It begins at approximately 660 °C and ends at about 500 °C. In addition, the quantity of every phase was also determined by an analysis of the micrographs with the digital microscope and the SEM. Using the image analysis software ImageJ on the micrographs, quantitative measurements of the phases were carried out. In contrast to this SEM-image analysis, the proportion of each phase was calculated by relating the surface areas of the peaks. These areas were normalized by dividing them by their volumetric expansion due to the transformation from austenite to ferrite (3.6013 pct), bainite (3.8632 pct), or martensite (4.3909 pct).^[16] An average was taken for bainite, as the transformation of austenite to lower or upper bainite results in slightly different values of 3.9679 pct for lower bainite and 3.7584 pct for upper bainite.

III. RESULTS AND DISCUSSION

A. Determination of Phase Transformations

The $D\phi_y/DT$ curves for the austenitization temperatures of 800 °C and 900 °C and of the samples that were soaked within 10 seconds and quenched without an elongation are depicted in Figure 4. For the blue curves,

which represent the cooling curve and the $D\phi_y/DT$ curve for an austenitization temperature of 900 °C, a bainite start temperature (B_s) of 646 °C and a martensite start temperature (M_s) of 429 °C were detected. The finish temperature of the martensitic transformation (M_f) was 287 °C. Small amounts of bainite were detected. Compared to the determined CCT diagram of Reference 3, the B_s was about 100 °C, the M_s 19 °C, and the M_f 30 °C higher. For the green curves, which represent the cooling curve and the $D\phi_y/DT$ curve for an austenitization temperature of 800 °C, the B_s was at 659 °C and the M_s at 437 °C; M_f amounted to 267 °C. Compared to the strong deflection of the blue $D\phi_y/DT$ curve, the peaks of the green $D\phi_y/DT$ curve are less pronounced, which is why the analyses of the transformation start and finish temperatures of this curve were performed separately. At a cooling rate of about 23 K/s, the resulting microstructure should consist of martensite and bainite, with a high proportion of martensite according to Reference 3. The critical cooling rate necessary for a full hardening of the steel 22MnB5 varies between 25 and 30 K/s.^[2,17] For a cooling rate of 23 K/s, Schaper *et al.* determined an F_s of about 700 °C, an B_s of 610 °C, an M_s of 400 °C, and an M_f of 260 °C at a soaking time of 300 seconds.^[4] The results of References 3 and 4 showed different CCT diagrams for the same heat treatment parameters. One reason for this could be small differences in the chemical composition.

Figure 5 shows the results of the phase transformation measurements using high-temperature DIC for all specimens and investigated areas of interest. Sample P1, which was heat treated similarly to P2 but with a cooling rate of about 12 K/s (see Figure 5(a)), showed a 70 °C higher ferrite start temperature (F_s) and a 30 °C higher B_s for an austenitization temperature of 900 °C compared to the results of Reference 3. However, the CCT diagram determined in Reference 4, in which the specimens were heat treated similarly to Reference 3, showed F_s and B_s comparable to sample P1. An influence of the short time austenitization on the transformation start and finish temperatures could be initially precluded, but further investigations are necessary to verify this result. The highest difference between the determined transformation start and finish temperatures for the three areas of specimen P2 was below 2.5 pct. No significant influence of the austenitizing temperature on the transformation start and finish temperatures of specimen P2 could be determined. In contrast to this, a higher difference of up to 16 pct between the determined transformation start and finish temperatures was found for specimen P1. A high influence of the austenitizing temperature on the bainitic transformation could be determined due to the lower cooling rate compared to sample P2. At a lower austenitization temperature, the bainitic area was larger, which could be the result of undissolved carbides because of the intercritical austenitizing below the Ac_3 temperature and the short time austenitization.^[18]

Figure 6 shows the temperature–time curve and the $D\phi_y/DT$ curve for specimen P4, in which a thermo-mechanical treatment with a 10 pct elongation with

subsequent compressed air quenching was carried out after a soaking duration of 10 seconds.

At an austenitization temperature of 850 °C (blue curves), the $D\phi_y/DT$ curve showed a larger peak for ferritic transformation, and two small peaks for bainitic and martensitic transformations. The determined F_s was at 777 °C, B_s at 503 °C, M_s at 379 °C, and M_f at 259 °C. With a cooling rate of about 19 K/s, this area can be compared with the ones in specimen P2 (Figure 5(a)). It can be noted that the hot plastic deformation influenced the detectable phases, since no ferritic transformation was detected for sample P2 at the same austenitization temperature compared to specimen P4, which only had a slightly lower cooling rate. The $D\phi_y/DT$ curve for 800 °C also had three peaks, though they were slightly further to the left. Since the quenching was performed at a lower austenitization temperature, the phase transformations started earlier. An F_s of 780 °C, B_s of 516 °C, M_s of 361 °C, and M_f of 257 °C were determined for a cooling rate of about 19 K/s. Schaper *et al.* showed that, even at high cooling rates, ferritic transformation is induced at about 800 °C due to hot plastic deformation,^[4] which is consistent with the results obtained for specimen P4. Furthermore, they observed an increase in the F_s and a shift of the transformation to shorter times as a result of the hot plastic deformation. These findings in combination with a slightly lower cooling rate may be the reason for the strong ferrite peak in the investigated areas of specimen P4 compared to P2. Due to the hot plastic deformation, the start of the bainitic transformation of P4 is at a temperature more than 100 °C lower than the B_s of sample P2. A delayed bainitic transformation could be the reason for the lower B_s , which was also found in Reference 4 for a hot plastic deformation of 20 pct. In contrast, Nikraves *et al.*^[6] found that a hot plastic deformation of 40 pct led to an increase in the bainitic transformation start temperature and a shift of the bainitic area to shorter times. As the austenitization temperature decreased, the M_s of specimen P4 was lowered equally to the M_s of P1, which was not deformed (see Figures 5(a) and (b)). Due to the graded heating of the specimens, the plastic deformation of the specimens was also inhomogeneous. At an austenitization temperature of 900 °C, a higher strain is applied than in the other two areas of interest with lower austenitization temperatures. Specimen P3 showed up to 25 °C lower values for the F_s and up to 139 °C higher values for the B_s compared to P4 (see Figure 5(b)). Furthermore, sample P3 had an extended bainitic area at a cooling rate of 12 K/s, which was also found in Reference 4. Nikraves *et al.*^[6] reported that at cooling rates above 6 K/s, the microstructure has more bainite in the deformed condition than in the non-deformed state.

The rate of the bainite reaction is accelerated by the deformation during thermo-mechanical processing.^[19] In addition, there is an increased possibility for bainitic transformation at subgrains and grain boundaries created by the deformation.^[6] The displacing nature of the bainite transformation at some cooling rates is responsible for a mechanical stabilization of the austenite, which inhibits the formation of bainite.^[20] Another

Table II. Experimental Plan for the Thermo-Mechanical Treatment of Flat Steel Specimens

Sample	Maximum Austenitization Temperature (°C)	Elongation at Hot Deformation (Pct)	Thickness (mm)	Cooling Method	Soaking Time (s)
P1	900	0	2	ambient air	10
P2	900	0	2	compressed air	10
P3	900	10 pct	2	ambient air	10
P4	900	10 pct	2	compressed air	10
P5	900	20 pct	2	ambient air	10
P6	900	20 pct	2	compressed air	10
P7	900	20 pct	1.5	ambient air	300

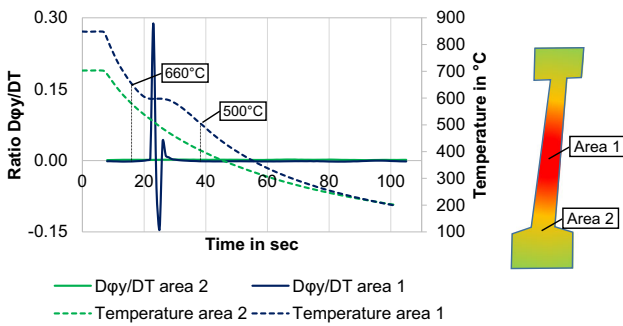


Fig. 3—Example of temperature–time curves and $D\phi_y/DT$ curves for two different areas of interest of a specimen cooled on ambient air.

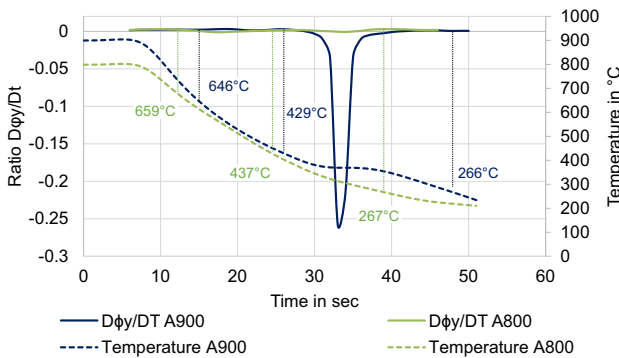


Fig. 4—Temperature–time curve and ratio of $D\phi_y/DT$ for specimen P2 with area 900 and area 800 plotted.

reason for the expansion of the bainitic area at higher cooling rates could be the mechanical stabilization of austenite, which causes a delay in the martensitic transformation.^[6]

The difference between the F_s for the three areas of interest was less than 2 pct for samples P3 and P4. An influence of the austenitization temperature on the F_s can therefore be ruled out.

P5 and P6, which were deformed up to an elongation of 20 pct, also have a higher F_s than P1 due to the hot plastic deformation (see Figures 5(a) and (c)). Specimen P5 reached an average F_s of 756 °C for all areas of interest, which is comparable to sample P3 with an average F_s of 757 °C. When comparing the results of samples P3 and P5 for an austenitization temperature of

900 °C, no significant differences in the transformation start and finish temperatures could be detected, with the exception of the B_s , which was 31 °C lower. For the other two areas of interest, the B_s was 22 and 9 pct lower than the B_s of specimen P3. The graded heating of specimen P5 resulted in a hot plastic deformation of 19 pct at 900 °C, 9 pct at 850 °C, and 3 pct at 800 °C. Due to the inhomogeneous strain distribution, valid comparisons between the two austenitization temperatures of 850 °C and 800 °C of samples P3 and P5 were not possible; the same applies to specimens P4 and P6. At an austenitization temperature of 900 °C, specimen P6 had a 109 °C higher B_s than P4 and a 17 °C lower B_s compared to the undeformed sample P2. Increasing the hot plastic deformation from 0 to 10 pct led to a shift of the B_s to longer times and a further increase from 10 to 20 pct led to a shift of the B_s to shorter times. These changes are due to the influence of hot forming on the transformation kinetics discussed in the previous paragraph.

In sample P7, a variation of the austenitization temperature at 300-second soaking time had no significant influence on the transformation start and finish temperatures (see Figure 6(d)). In contrast to sample P5, the uneven strain distribution due to the graded heat treatment did not affect the B_s and B_f . Samples P5 and P7, where solely the soaking time was varied, differed only in their B_s and M_f . The reason for deviations in the B_s could be the more homogeneous distribution of alloying elements, especially carbon, as a result of the longer soaking time. These results showed that the soaking time had a more significant influence on the B_s than the austenitization temperature.

For samples P1, P3, P5, and P7, the $D\phi_y/DT$ curves fluctuated between the M_s and the end of the measurement with only smaller peaks, which made it difficult to determine the M_f . The reason for this fluctuation could be self-tempered martensite, a result of the fact that these four specimens were cooled in ambient air at a relatively low rate of about 12 K/s. According to Reference 21, relatively low cooling rates during quenching generally lead to the occurrence of self-tempered martensite. The measuring range of the thermal imaging camera does not allow further investigations regarding a possible end of the oscillation.

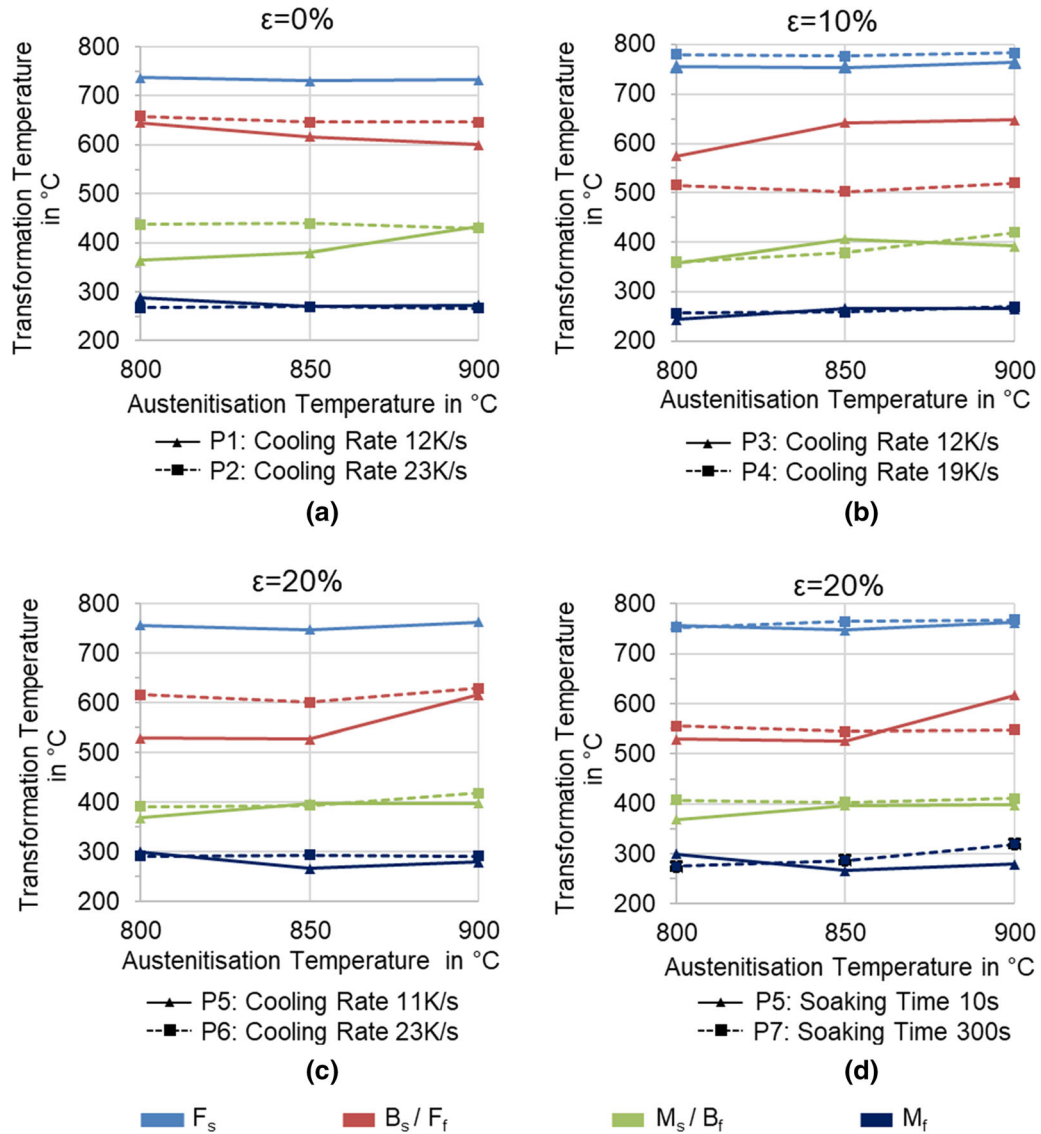


Fig. 5—Influence of hot deformation (a through c) and soaking time (d) on the temperature range of phase transformations (P1 to P6 with 10-s soaking time and P7 with 300-s soaking time).

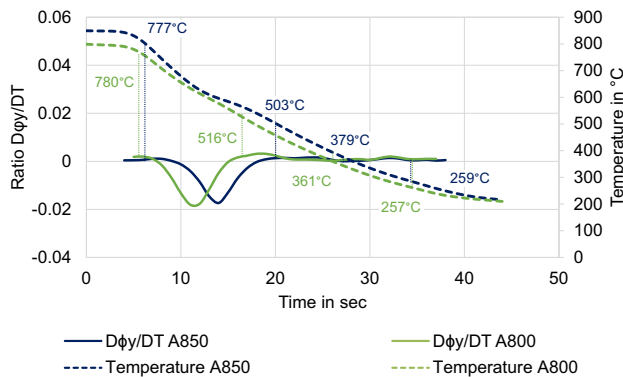


Fig. 6—Temperature–time curve and ratio of $D\phi_y/DT$ for specimen P4 with area 850 and area 800 plotted.

B. Micrograph and Hardness Investigations

The micrographs and SEM images for the two opposite areas of interest of specimen P2 are depicted in Figure 7. According to Reference 22, a martensitic microstructure reaches a very light or white color after a LePera etchant. Due to the similar carbon content, an austenitic microstructure has the same color. Furthermore, the self-tempered martensite should take on a brown, bainite a beige, and ferrite a gray-blue color after the LePera etching.

Figure 7(a) shows a mostly light-colored microstructure with lancets, which, in combination with the SEM images of sample P2 in the area austenitized at 900 °C (see Figure 7(b)), indicates a mostly martensitic microstructure. While the beige grains imply a small amount of bainite, the hardness of about 440 HV1

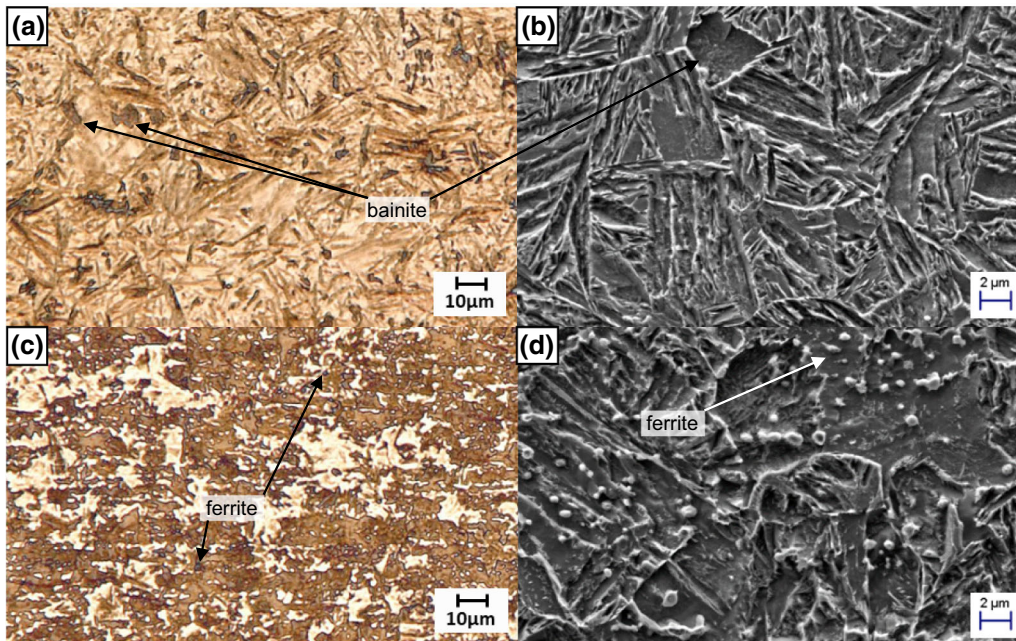


Fig. 7—Micrographs (LePera etchant) and SEM images of different areas of interests of the specimen P2 (a) and (b) correspond to 900 °C, whereas (c) and (d) correspond to 800 °C.

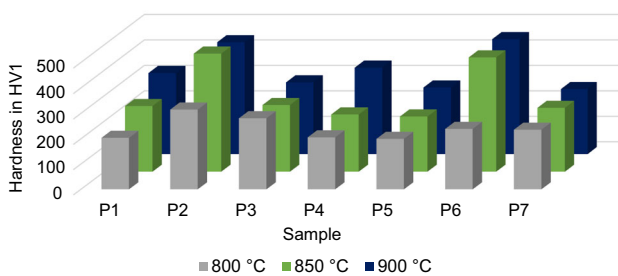


Fig. 8—Hardness of the investigated areas for all tested specimens.

(Figure 8) proves an almost fully martensitic microstructure in this area. The analysis of the phase fractions for the area of P2 austenitized at 900 °C showed a proportion of 5 pct bainite and 95 pct martensite (see Figure 9(a) dashed lines), which correlates with the hardness determined. Figure 7(c) reveals a different structure in the area austenitized at 800 °C, where the large light grains represent martensite and the small white particles carbides. According to the SEM analysis (7d), the beige-brown matrix corresponds to bainite. Since the graded austenitization was performed in the intercritical austenitization temperature range, the microstructure contains some retained ferrite grains of about 2 microns, which were visible on the SEM images in zones with undissolved carbides. Additionally, small gray ferrite grains can be found in Figure 7(c). The hardness in this area amounted to 315 HV1 (see Figure 8), which correlates with the determined phase fractions of 7 pct ferrite, 63 pct bainite, and 30 pct martensite as well as the micrograph.

Compared to the SEM image 7(b), a high number of undissolved carbides are visible in 7d. Since cooling was initiated below the A_{c1} temperature, the inhomogeneous

austenite exhibits an uneven distribution of the alloying elements, which is why low-carbon areas occur. While martensite usually forms in the vicinity of carbides, low-carbon regions generally convert to bainite due to an insufficient carbon content within the metallic matrix.^[23,24] In addition, the soaking time of 10 seconds was too short for a complete dissolution of the carbides, which contributed to the inhomogeneous carbon distribution. After quenching, low-carbon regions transform into bainite or low-carbon martensite.^[25] Grydin *et al.* found that in contrast to a conventionally austenitized material, the microstructure of a short austenitized material consists of ferrite, bainite, martensite, retained austenite, and a small amount of carbides.^[18] These are the reasons for the higher bainite content and the slightly higher B_s -temperature after austenitizing at 800 °C compared to the areas austenitized at 850 °C or at 900 °C.

Figure 10 shows digital light microscope and SEM images for two areas of interest of P4 austenitized at 850 °C and 800 °C. The micrograph in Figure 10(a) demonstrates a mostly ferritic microstructure (gray matrix) in the area of the steel that was thermo-mechanical treated at 850 °C. Within this gray matrix, beige-orange colored grains are visible, which correspond to bainite according to the SEM analysis. Small amounts of martensite are evident on the light microscope and SEM images. The hardness of about 226HV1 in this area (see Figure 8) is proof of a high ferrite content.

Compared to the micrograph in Figure 10(a), Figure 10(c) shows a smaller amount of martensite, which is equivalent to the area heated to 800 °C. The color of the matrix changed to a mixture of gray and purple, which is the result of a different intensity of the etching. The contrast between ferrite and bainite is still

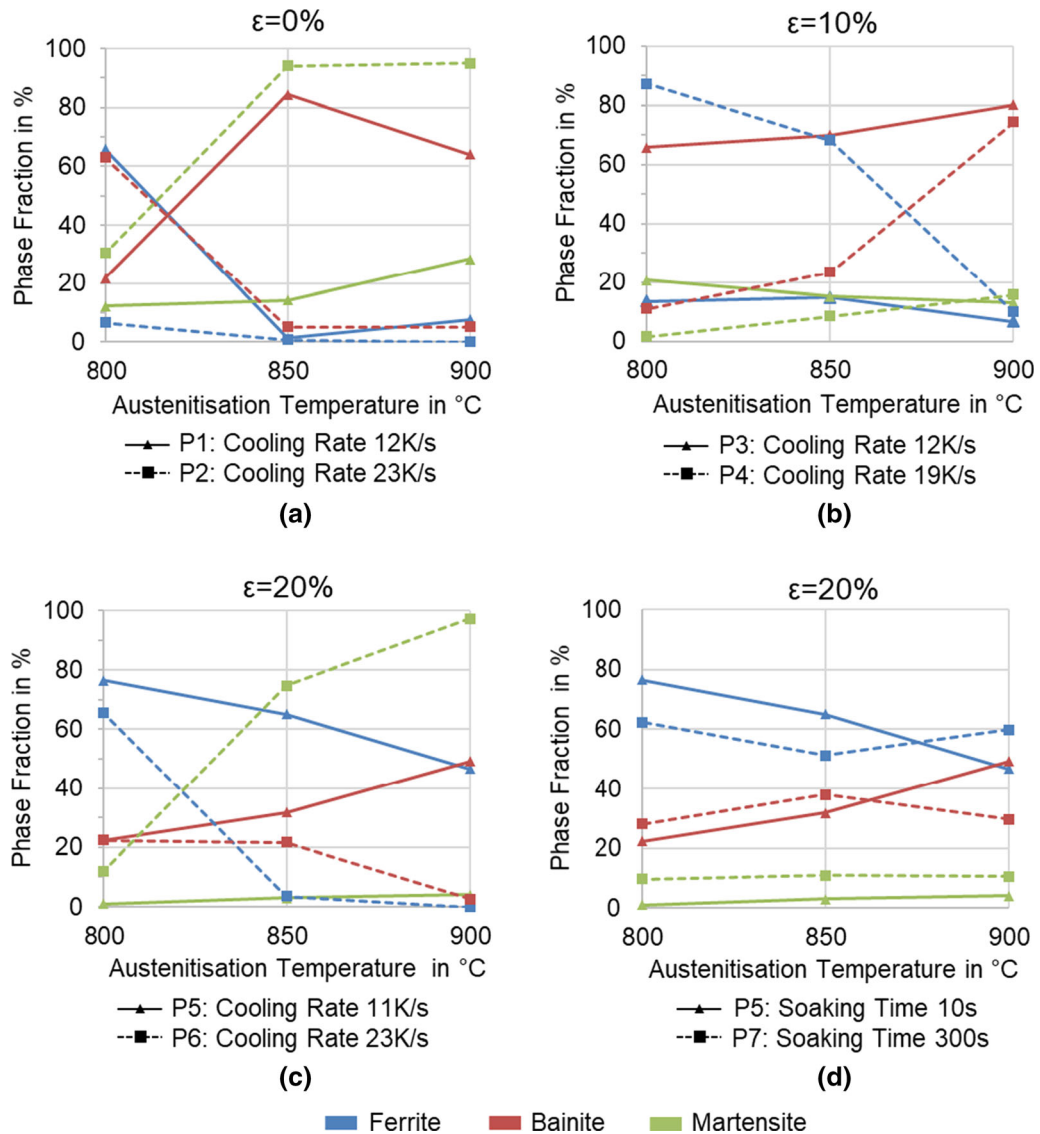


Fig. 9—Influence of hot deformation (*a* to *c*) and soaking time (*d*) on the phase fractions according to the microstructural characterization (P1 to P6 with 10-s soaking time and P7 with 300-s soaking time).

sufficient, with the beige-brown areas representing the bainitic phase. The hardness of 206 HV1 confirms a high amount of ferrite (87 pct) in this area (see Figures 8 and 9(b) dashed lines).

The hot plastic deformation of P4 at an austenitization temperature of 900 °C and a plastic deformation of 10 pct lead to a higher amount of bainite compared to the undeformed P2. A further increase in hot plastic deformation to 20 pct (P6) resulted in an almost identical phase content as in sample P2 (see Figure 9(c)). The changed transformation kinetics combined with the difference of about 4 K/s in the cooling rate could be the decisive factor for the shift of the dominant phase of P4.

Specimen P3 had a higher martensite volume fraction and thus a 6 pct higher hardness at an austenitization temperature of 800 °C than at 850 °C (see Figure 9(b)). One reason for this is the inhomogeneous strain distribution, the elongation achieved at 800 °C being

lower than at 850 °C. As already mentioned, the hot deformation shortened the start of the ferritic and bainitic transformations, which in turn led to the higher amount of martensite at an austenitization temperature of 800 °C.

P7 exhibited a higher ferrite and martensite volume fraction compared to P5 at an austenitization temperature of 900 °C (see Figure 9(d)). The hardness of both areas was almost equal. One explanation for the high bainite volume fraction of P5 within this area could be the short time austenitization. The dissolution of cementite or other carbides of the initial structure was incomplete during the short time austenitization of the steel. Since the carbon diffusion process is time-dependent, there was not enough time for completion. The resulting inhomogeneous carbon distribution then led, as mentioned above, to the formation of carbon-rich and carbon-poor regions, which could be the reason for the gradient of carbon in the austenite, and the resulting

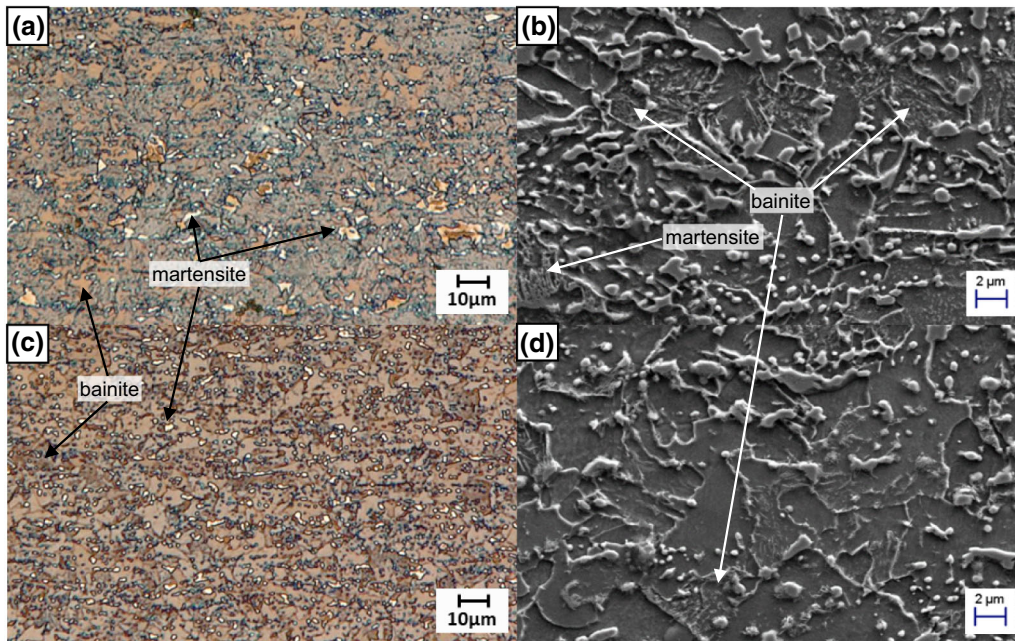


Fig. 10—Micrographs (LePera etchant) and SEM images of different areas of interests of the specimen P4 (a) and (b) correspond to 850 °C, whereas (c) and (d) correspond to 800 °C.

gradation of the microstructure. A microstructure consisting of ferrite, bainite, martensite and not completely dissolved carbides is formed during steel cooling.^[18,26]

Furthermore, alloying elements such as manganese or chromium reduce the critical cooling rate. In microscopically small areas where high amounts of these alloying elements are present, for example around dissolved carbides, martensite is formed. In regions where only few of these elements are available, austenite converts to ferrite and bainite. Thus, both the beginning of the bainitic transformation at higher temperatures and the inhomogeneous distribution of alloying elements could be the reason for the higher bainite content after short austenitization. Furthermore, the austenitization temperature has no significant influence on the phase content and therefore the hardness of specimen P7.

In contrast to the results of Reference 9, where the cooling rate reached 50 K/s, no undissolved pearlite could be found within the investigated areas of all samples at austenitization temperatures of 800 °C and 850 °C.

Since the critical cooling rate was not reached in any test, no 100 pct martensitic microstructure occurred. The hardness values for all investigated areas correlated with the determined phase compositions.

C. Evaluation of the Phase Content from High-Temperature DIC Curves

Two different methods were used to determine the phase compositions of each specimen. Examples of the results are given in Figures 11(a) through (d). Both

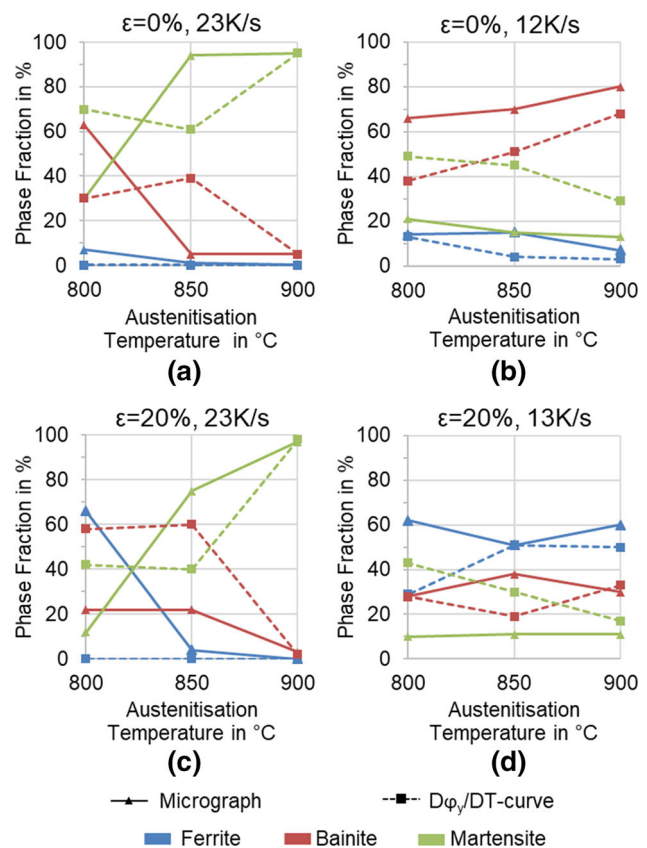


Fig. 11—Comparison between the determination of the phase contents by analysis of the micrographs and $D\phi_v/DT$ curve for different cooling rates: (a) sample P2, (b) sample P3, (c) sample P6, (d) sample P7.

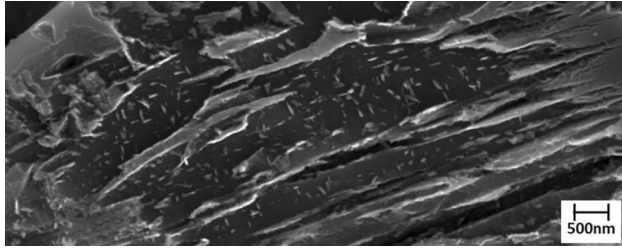


Fig. 12—Self-tempered martensite of specimen P7 within the area of 900 °C.

methods yielded identical results for the specimens P2 and P6 within the areas austenitized at 900 °C (see Figures 11(a) and (c)). With the new method, in which the ratio of the surface areas of the peaks is calculated, a high accuracy can be achieved for high cooling rates of about 23 K/s. At lower cooling rates of about 12 K/s, as for example with specimen P3 and P7, a too high martensite content is determined at the same austenitization temperature (see Figures 11(b) and (d)). The oscillation of the $D\phi_y/DT$ curves after the M_s made it difficult to determine the M_f , as mentioned in 3.1. One cause for the detected fluctuation is the occurrence of self-tempered martensite, which can be seen in Figure 12. These martensite laths consist of fine precipitates that are randomly oriented and resemble ϵ carbides ($Fe_{2.3}C$) or η carbides (Fe_2C). They normally precipitate from the martensite during the first tempering stage.^[18,21,27]

The results for lower austenitization temperatures are distorted due to the presence of untransformed retained ferrite, as cooling was initiated below the Ac_3 temperature. Furthermore, the curves in Figures 4 and 6 showed that the size of the peaks provides information about the dominant phase and therefore the hardness can be estimated. For example, the blue $D\phi_y/DT$ curve in Figure 4 shows a very strong peak for the martensitic transformation. This area had a high martensite content and therefore a high hardness.

IV. CONCLUSIONS

In this paper, the effects of different austenitization temperatures, hot deformation, soaking duration, and cooling conditions on phase transformation kinetics and the resulting phase composition were investigated. A new contactless characterization method was used to determine the phase transformations. The results can be summarized as follows:

1. With the contactless characterization method, phase transformations could be detected and the start and finish transformation temperatures for every phase could be determined. However, the M_f was difficult to determine for low cooling rates of about 12 K/s (ambient air), due to the self-tempering of martensite and the limited measuring range of the thermal imaging camera.

2. A lower austenitization temperature resulted in a reduced hardness, since less martensite and a higher proportion of ferrite and bainite are present in undeformed specimens. Furthermore, the undeformed samples showed that the influence of the austenitization temperature on the bainitic and martensitic transformation was higher at a low cooling rate of 12 K/s than at a high cooling rate of 23 K/s. In deformed samples, the austenitization temperature influenced the martensitic and especially the bainitic transformation. At austenitization temperatures below 900 °C, a high number of undissolved carbides were visible on the SEM images. One reason for these effects could be the short soaking time, which led to an inhomogeneous distribution of the alloying elements and undissolved carbides.
3. Hot deformation led to a shift of the F_s to higher temperatures and shorter times. Increasing the total hot deformation from 10 to 20 pct led to an increase of the F_s for higher cooling rates. The effect of the hot deformation on the bainitic transformation was highly variable, as an increase of the hot plastic deformation from 0 to 10 pct resulted in a shift of the bainitic transformation to longer times and a further increase of it from 10 to 20 pct resulted in a shift to shorter times. The graded thermo-mechanical processing led to an uneven strain distribution within the specimens and resulted in a higher hardness at the lowest austenitization temperature of 800 °C, as the strain was lowest in this area (see specimen P3). This must be taken into account when setting a mixed microstructure for components produced by graded thermo-mechanical processing.
4. The higher soaking time of 300 seconds compared to the short time austenitization of 10 seconds resulted in uniform transformation start and finish temperatures at different austenitization temperatures. The reason for this was an even distribution of the alloying elements in the iron.
5. The volume of every phase could be determined by relating the surface areas of the peaks. However, an exact determination of the phase contents was only possible at high cooling rates after a complete austenitization of the samples. Especially for an austenitization below the Ac_3 temperature, incorrect phase results were calculated because of the retained ferrite. However, the size of the peaks provided information about the dominant phase of the thermo-mechanically treated steel.

In summary, this study showed that the investigation of phase transformation kinetics using the contactless characterization method and the determination of CCT and deformed CCT diagrams is possible with a reduced experimental effort and a small number of specimens. The influence of different austenitization temperatures on the transformation kinetics can be examined using one specimen.

ACKNOWLEDGMENTS

The authors thank the German Research Foundation (DFG) for financial support of the Project SCHA 1484/38-1.

FUNDING

Open Access funding provided by Projekt DEAL.

OPEN ACCESS

This article is licensed under a Creative Commons Attribution 4.0 International License, which permits use, sharing, adaptation, distribution and reproduction in any medium or format, as long as you give appropriate credit to the original author(s) and the source, provide a link to the Creative Commons licence, and indicate if changes were made. The images or other third party material in this article are included in the article's Creative Commons licence, unless indicated otherwise in a credit line to the material. If material is not included in the article's Creative Commons licence and your intended use is not permitted by statutory regulation or exceeds the permitted use, you will need to obtain permission directly from the copyright holder. To view a copy of this licence, visit <http://creativecommons.org/licenses/by/4.0/>.

REFERENCES

1. R. George, A. Bardelcik, and M.J. Worswick: *J. Mater. Process. Technol.*, 2012, vol. 212 (11), pp. 2386–99, <https://doi.org/10.1016/j.jmatprotec.2012.06.028>.
2. M. Merklein, M. Wieland, M. Lechner, S. Bruschi, and A. Ghiotti: *J. Mater. Process. Technol.*, 2016, vol. 228, pp. 11–24, <https://doi.org/10.1016/j.jmatprotec.2015.09.023>.
3. M. Naderi, A. Saeed-Akbari, and W. Bleck: *J. Mater. Sci. Eng. A*, 2008, vol. 487 (1–2), pp. 445–55, <https://doi.org/10.1016/j.msea.2007.10.057>.
4. M. Schaper, G. Gershteyn, O. Grydin, D. Fassmann, Z. Yu, and F. Nürnberger: *5. Erlanger Workshop Warmblechumformung*, vol. 2010, pp. 141–60.
5. H. Järvinen, M. Isakov, T. Nyssönen, M. Järvenpää, and P. Peura: *J. Mater. Sci. Eng. A*, 2016, vol. 676, pp. 109–20, <https://doi.org/10.1016/j.msea.2016.08.096>.
6. M. Nikravesh, M. Naderi, G.H. Akbari, and W. Bleck: *Mater. Des.*, 2015, vol. 84, pp. 18–24, <https://doi.org/10.1016/j.matdes.2015.06.108>.
7. J. Min, J. Lin, and Y.A. Min: *J. Mater. Process. Technol.*, 2013, vol. 213 (6), pp. 818–25, <https://doi.org/10.1016/j.jmatprotec.2012.12.012>.
8. Z. Shi, K. Liu, M. Wang, J. Shi, H. Dong, J. Pu, B. Chi, Y. Zhang, and L. Jian: *J. Mater. Sci. Eng. A*, 2012, vol. 535, pp. 290–96, <https://doi.org/10.1016/j.msea.2011.12.088>.
9. J. Zhou, B.-Y. Wang, M.-D. Huang, and D. Cui: *Int. J. Miner. Metall. Mater.*, 2014, vol. 21 (6), pp. 544–55, <https://doi.org/10.1007/s12613-014-0940-7>.
10. T. Nishibata and N. Kojima: *J. Alloys Compd.*, 2013, vol. 577, pp. 549–54, <https://doi.org/10.1016/j.jallcom.2011.12.154>.
11. A. Grajcar, W. Zalecki, P. Skrzypczyk, A. Kilarski, A. Kowalski, and S. Kołodziej: *J. Therm. Anal. Calorim.*, 2014, vol. 118 (2), pp. 739–48, <https://doi.org/10.1007/s10973-014-4054-2>.
12. M. Gojic, M. Suceska, and M. Rajic: *J. Therm. Anal. Calorim.*, 2004, vol. 75, pp. 947–56.
13. J. Zachrisson: *Lulea University of Technology—Department of Applied Physics and Mechanical Engineering, Master Thesis*, 2012, pp. 1–3.
14. R. Kumar and H.K. Arya: *J. Mater. Sci. Eng.*, 2013, vol. 03 (02), pp. 1–4, <https://doi.org/10.4172/2169-0022.1000138>.
15. F.S. LePera: *JOM*, 1980, vol. 32 (3), pp. 38–39, <https://doi.org/10.1007/BF03354553>.
16. G.E. Totten, M.A.H. Howes, and T. Inoue: *Handbook of Residual Stress and Deformation of Steel*, ASM International, Materials Park, 2002, pp. 249–50.
17. M. Naderi: *Hot Stamping of Ultra High Strength Steels*, Dissertation, 2007, pp. 76–77.
18. O. Grydin, A. Andreiev, M.J. Holzweißig, C.J. Rüsing, K. Duschik, Y. Frolov, and M. Schaper: *J. Mater. Sci. Eng. A*, 2019, vol. 749, pp. 176–95, <https://doi.org/10.1016/j.msea.2019.02.025>.
19. H.K.D.H. Bhadeshia: *Bainite in Steels: Transformations, Microstructure and Properties*, 2nd ed., IOM Communications, London, 2001, pp. 203–13.
20. H.K.D.H. Bhadeshia: *Mater. Sci. Technol.*, 1999, vol. 15 (1), pp. 22–29, <https://doi.org/10.1179/026708399773002773>.
21. G.R. Speich and W.C. Leslie: *Metall. Trans.*, 1972, vol. 3 (5), pp. 1043–54, <https://doi.org/10.1007/BF02642436>.
22. M. Pranger: *Vergleich der Mikrostruktur ausgewählter hochfester Schweißungen*, Diploma Thesis, 2017, pp. 46–47.
23. O. Grydin, F. Nuernberger, Y. Zou, M. Schaper, and A. Brosius: *Steel Res. Int.*, 2014, vol. 85 (9), pp. 1340–47, <https://doi.org/10.1002/srin.201300420>.
24. A. Andreiev, O. Grydin, and M. Schaper: *A Rapid Heating Method for Press Hardening Processing*, Springer International Publishing, Cham, 2017, pp. 723–36.
25. T. Lolla, G. Cola, B. Narayanan, B. Alexandrov, and S.S. Babu: *Mater. Sci. Technol.*, 2011, vol. 27 (5), pp. 863–75, <https://doi.org/10.1179/174328409X433813>.
26. A. Andreiev, O. Grydin, and M. Schaper: *Steel Res. Int.*, 2016, vol. 87 (12), pp. 1733–41, <https://doi.org/10.1002/srin.201600086>.
27. L. Cheng, C.M. Brakman, B.M. Korevaar, and E.J. Mittemeijer: *Metall. Trans.*, 1988, vol. 19 (10), pp. 2415–26, <https://doi.org/10.1007/BF02645469>.

Publisher's Note Springer Nature remains neutral with regard to jurisdictional claims in published maps and institutional affiliations.